Bulletin of Engineering Geology and the Environment (2020) 79:789–810
https://doi.org/10.1007/s10064-019-01596-x

ORIGINAL PAPER

Modification of the rock mass rating system (RMR_{mbi}) considering three-dimensional rock block size

Qingfa Chen[1] · Tingchang Yin[1]

Received: 24 March 2019 / Accepted: 13 August 2019 / Published online: 23 August 2019

Abstract

Traditional measurements of block size (or degree of jointing), such as the rock quality designation (*RQD*), are questionable due to certain theoretical limitations, including orientation bias and their weakness in considering the joint persistence and three-dimensional shapes of block sizes. This may lead to inaccurate characterizations of rock mass structures and unreliable classification of rock mass qualities. The modified blockiness index (MB_i) is a three-dimensional measurement of block size which was developed to overcome these problems. In this study, correlations between MB_i and several traditional block size measurements were assessed; based on the MB_i, the rock mass rating (*RMR*) system was modified, and this version was termed RMR_{mbi}. In the first part of this work, multiple simulated experiments were conducted using the GeneralBlock software program and 3DEC (three-dimensional distinct element code), and a large volume of MB_i, *RQD*, joint frequency (*JF*) and volumetric joint count (J_v) values (artificial data sets) were obtained; subsequently, the correlations between MB_i and *RQD*, *JF* and J_v were assessed. In the second part, the combined use of *RQD* and *JF* in the *RMR* system was replaced with MB_i, and hence, the RMR_{mbi} system was developed; based on the artificial data sets, the viability of RMR_{mbi} was preliminarily supported. At the end of this study, the correlations between MB_i and *RQD*, *JF* and J_v were verified based on actual data; the RMR_{mbi} was applied to real cases, and a comparison between RMR_{mbi} and *RMR* was conducted. The results showed that (i) the MB_i can capture the influence of joint persistence; (ii) the RMR_{mbi} system can overcome the theoretical limitations caused by *RQD* and *JF*; and (iii) simulated experiments showed that the RMR_{mbi} values are more reliable, thus validating the accuracy of RMR_{mbi} and revealing its great potential for future application.

Keywords Modified blockiness index · Block size measurements · Rock mass rating · RMR_{mbi}

Abbreviations

3DEC	Three-dimensional distinct element code
3DJN	Three-dimensional joint network model
A	Rotation matrix
COV	Coefficient of variation
d_3	Three-dimensional joint density
JF	Joint frequency
JN	Joint set number
JO	Joint orientation
JP	Joint persistence
JS	Joint spacing
J_v	Volumetric joint count
MAPE	Mean absolute percentage error
MB_i	Modified blockiness index
REV	Representative elementary volume
R_M	The rating of MB_i in the RMR_{mbi} system
RMR	Rock mass rating system
RMR_{mbi}	A modified *RMR* system based on the MB_i
RMSE	Root-mean-square error
RQD	Rock quality designation
R_{RQD+JF}	The ratings of *RQD* plus *JF* in the *RMR* system
VIF	Variance inflation factor

✉ Qingfa Chen
chenqf@gxu.edu.cn

Tingchang Yin
yintingchang@foxmail.com

[1] College of Resources, Environment and Materials, Guangxi University, Nanning, Guangxi 530004, People's Republic of China

Introduction

Rock mass is a type of discontinuous material that often contains a variety of joints, which discretize the rock mass into blocks of various sizes and shapes

(Palmstrom 2005; Xia et al. 2016; Yarahmadi et al. 2018). The quantity and sizes of blocks within rock mass (or degree of blockiness) have a major controlling influence on the quality and stability of rock masses. Accurate measurement of block size is a basic task in rock mass characterization and classification, and can also provide robust data for designing rock engineering structures (Celada et al. 2014).

Over the past several decades, a large number of block size measurements have been proposed. Some existing measurements are listed in Table 1. In this table, all the three-dimensional measurements are indirect, because rock mass structure cannot be directly examined in three dimensions (Shang et al. 2018), and these three-dimensional measurements are basically performed from the joint data acquired from rock exposure. In addition, joint frequency (*JF*) is essentially identical to joint spacing (*JS*), and the same is true for volumetric joint count (J_v) and P30.

Table 2 Jointing classes based on MB_i (Chen et al. 2018)

MB_i	Jointing or blockiness degree
0–7%	Integrated or non-blockiness
7–27%	Relatively integrated or slight blockiness
27–55%	Poorly integrated moderate blockiness
55–85%	Relatively fractured or blockiness
85–100%	Fractured or serious blockiness

Actually, only a few of these measurements have been widely accepted, including the *RQD*, *JF*, and J_v. The *RQD* has gained wide acceptance and application compared to the other two indices. In civil and mining engineering worldwide, borehole penetrations occur every day, and professionals always record the degree of rock mass jointing in the form of *RQD* (Zhang 2016). Also, many rock mass quality classification systems include *RQD* as a basic input parameter, for example, the

Table 1 An overview of existing measurements of block size (or degree of blockiness)

Measurement	Definition	Type
Rock quality designation (*RQD*) (Deere et al. 1967)	The percentage of intact core pieces longer than 100 mm in the total length of core	One-dimensional; measured on drill cores or scanlines; direct
RQD/*JN* (Barton et al. 1974)	The quotient *RQD*/*JN* (*JN* denotes the number of joint sets), which is a crude measure of block size	One-dimensional; measured on drill cores or scanlines; direct
Joint frequency (*JF*) (ISRM 1978)	The number of joints per meter	One-dimensional; measured on scanlines; direct
Joint spacing (*JS*) (ISRM 1978)	The perpendicular distance between two joints within a joint set, or the inverse of *JF*	One-dimensional; measured on scanlines; direct
Volumetric joint count (J_v) (Palmstrom 1982)	The number of joints intersecting a volume of 1 m^3	Three-dimensional; measured on rock surface; indirect
Block volume (V_b) (Palmstrom 1996)	Block sizes, which can be estimated by J_v	Three-dimensional; measured on rock surface; indirect
P10 (Dershowitz et al. 2003)	Number of joints per unit length	One-dimensional; measured on drill cores or scanlines; direct
P11 (Dershowitz et al. 2003)	Length of joints per unit length	One-dimensional; measured on drill cores or scanlines; direct
P20 (Dershowitz et al. 2003)	Number of joints per unit area	Two-dimensional; measured on rock surfaces; direct
P21 (Dershowitz et al. 2003)	Length of joints per unit area	Two-dimensional; measured on rock surfaces; direct
P22 (Dershowitz et al. 2003)	Area of joints per unit area	Two-dimensional; measured on rock surfaces; direct
P30 (Dershowitz et al. 2003)	Number of joints per unit volume	Three-dimensional; measured on rock surface; indirect
P32 (Dershowitz et al. 2003)	Area of joints per unit volume	Three-dimensional; measured on rock surface; indirect
P33 (Dershowitz et al. 2003)	Volume of joints per unit volume	Three-dimensional; measured on rock surface; indirect
Modified blockiness index (MB_i) (Xia et al. 2015; Chen et al. 2018)	Blockiness level of a jointed rock mass (for more details please see Section 2)	Three-dimensional; measured on rock surface; indirect

Table 3 Joint geometrical parameters used to construct *3DJN* models (Xia et al. 2015)

Group no.	1	2	3
Distribution type of trace length	Log-normal	Log-normal	Log-normal
Joint trace standard deviation (m)	5.982	5.545	7.323
Distribution type of joint orientation	Fisher	Fisher	Fisher
κ for Fisher	9.50	7.80	10.49
Average dip direction (°)	80.07	261.77	355.76
Average dip angle (°)	40.22	47.52	71.70

geomechanics classification system/rock mass rating system (*RMR*) (Bieniawski 1989), tunneling quality index (*Q*-system) (Barton et al. 1974) and the quantified version of the Geological Strength Index chart (*GSI*) (Hoek and Diederichs 2013). The use of *JF* and J_v is also popular. In the *RMR* system, *JF* has a weighting "score" of 20 points, which is used together with *RQD* to quantify the degree of rock mass jointing; notably, in the updated version of the *RMR* system (Celada et al. 2014), the combined use of *RQD* and *JF* was replaced by the sole use of *JF*, but this version is controversial (Koutsoftas 2017). The J_v is often used in conjunction with the Rock Mass index (*RMi*) (Palmstrom 1996), and in some Chinese geotechnical codes (PRC Ministry of Construction 1995), the intactness index of rock mass (K_v) (Liu et al. 2017) can be estimated using J_v. It should be noted that the previous findings are reviewed only from the perspective of the essential concepts of these indices; some works in which certain techniques such as three-dimensional point cloud (Riquelme et al. 2016) and discrete fracture network (Zhang et al. 2013) were employed to determine the *RQD*, *JF* or J_v value are not discussed in this study.

However, various researchers (Palmstrom 2005; Zhang et al. 2012; Chen et al. 2019) have noted that the three measurements (i.e., *RQD*, *JF* and J_v) are limited. For example, two major criticisms of *RQD* are that *RQD* values are very sensitive to the scanline or borehole direction, and that *RQD* counts only the core pieces longer than 100 mm and therefore cannot effectively differentiate rock masses with various structures. These two shortfalls have become the basis for arguments against the use of the *RQD* in rock mass classification systems (Pells et al. 2017). The other two indices also suffer from limitations: *JF* is also orientation-dependent, and joint persistence is ignored in the J_v method (Lin 2008). Actually, many block size measurements and rock mass quality classification systems fail to consider joint persistence (Kim et al. 2007). In addition, Hoek and Diederichs (2013) reported that some traditional measurements of the degree of rock mass jointing, including *RQD*, *JF* and J_v, cannot capture the effect of block scale.

Other measurements of block size were not mentioned, such as the weighted joint density (*WJD*) (Terzaghi 1965), *RQD*/*JN* (Barton et al. 1974) (*RQD*/*JN* denotes the *RQD* value divided by the joint set number) and block volume (V_b) (Palmstrom 2005). This is due to the following: (i) the *WJD* is, in fact, a correct approach for joint data, which is mainly used to remedy the one-dimensional joint density for borehole orientation bias (Terzaghi 1965); (ii) the *RQD*/*JN* is slightly unreliable, because the determination of the *JN* is often subjective in nature (Grenon and Hadjigeorgiou 2003); and (iii) the V_b is an interpretation of J_v (Palmstrom 2005).

Inaccurate measurement of block size (or degree of rock mass jointing) may result in unreliable classification of rock mass quality (Palmstrom 2005; Aydan et al. 2014). Therefore, in this study, the modified blockiness index (MB_i) is introduced (for details, see Section 2), and an attempt has been made to

Table 4 Classification of joint spacing and persistence (ISRM 1978) and chosen values

Classification of joint spacing							
Interval	> 6 m	2–6 m	0.6–2 m	0.2–0.6 m	0.06–0.2 m	0.02–0.06	< 0.02 m
Chosen value (m)	7	4	0.9, 1.3, 1.7, 2	0.3, 0.4, 0.5 and 0.6	0.08, 0.09, 0.13, 0.17, 0.2	0.04, 0.06	0.01
Classification of joint persistence							
Interval	> 20 m	10–20 m		3–10 m	1–3 m	0–1 m	
Chosen value (m)	30, 40	15, 20		5, 10	2 and 3	0.5, 1	

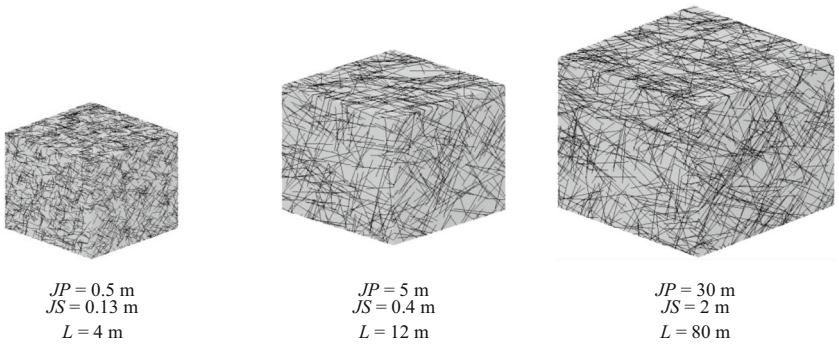

Fig. 1 Some *3DJN* models (note that *JP* denotes the joint persistence, *JS* denotes the joint spacing, and *L* denotes the side length of the model)

incorporate the MB_i into the *RMR* system. The study consists of two main parts: (i) correlations of MB_i with *RQD*, *JF* and J_v are evaluated; and (ii) a modified *RMR* system (RMR_{mbi}) with a great application potential is developed and its viability analyzed. To consider all possible cases, the study was carried out based on multiple simulated experiments and some real engineering projects. In addition, multiple simulated experiments were conducted using the GeneralBlock program (a *3DJN* model generator) (Xia et al. 2016) and 3DEC (three-dimensional distinct element code) (Itasca 2013) together.

Outline of the modified blockiness index (MB_i)

Joints intersect rock mass in complicated three-dimensional patterns; however, traditional measurements of block size are often performed in one or two dimensions, and they are also unable to consider the influence of joint persistence and block scale. The modified blockiness index (MB_i), proposed by Xia et al. (2015) and revised by Chen et al. (2018), is capable of overcoming these difficulties. The MB_i is a three-dimensional measurement that enables the quantification of the block size distribution of a given rock mass, and its calculation is based on the three-dimensional join network model (*3DJN* model) generated by stochastic and/or deterministic joints. MB_i value can be calculated by

$$MB_i = B_1 + \frac{1}{2}B_2 + \frac{1}{3}B_3 + \frac{1}{4}B_4 + \frac{1}{5}B_5 \quad (1)$$

where B_1, B_2, B_3, B_4 and B_5 are the ratios of blocks in the ranges of 0–0.008 m^3, 0.008–0.03 m^3, 0.03–0.2 m^3, 0.2–1.0 m^3, and > 1.0 m^3, respectively, to the total rock mass volume, and the fractions (i.e., 1, 1/2, 1/3, 1/4 and 1/5) are the empirical scale effect coefficients, which are determined based on engineering practice (Wang et al. 2010; Chen et al. 2018). When the MB_i value is close to 1, it suggests that the rock mass is very fractured; when the MB_i value is close to 0, it indicates a very low degree of rock mass jointing. The suggested jointing classes based on MB_i are presented in Table 2.

In fieldwork, the MB_i associated with a given rock mass can be determined based on the following steps: (i) obtaining joint measurement data, including joint orientation, trace length and joint density; (ii) demarcating statistically homogeneous structural domains: generally, the domains can be identified using joint orientation data, together with various statistical methods, e.g., Chi-square test (Miller 1983; Martin and Tannant 2004; Li et al. 2014); (iii) establishing a three-dimensional joint network model; (iv) identifying the sizes of all blocks inside the rock mass model; and (v) calculating the MB_i value using Eq. (1). Steps (iii) and (iv) can be carried out using GeneralBlock.

In essence, the MB_i concept can be treated approximately as an extension of *RQD* and V_b, namely, all the MB_i, *RQD* and V_b are direct representations of the blockiness of rock mass, which are different from *JF* and J_v. In other words, MB_i, *RQD* and V_b all consider

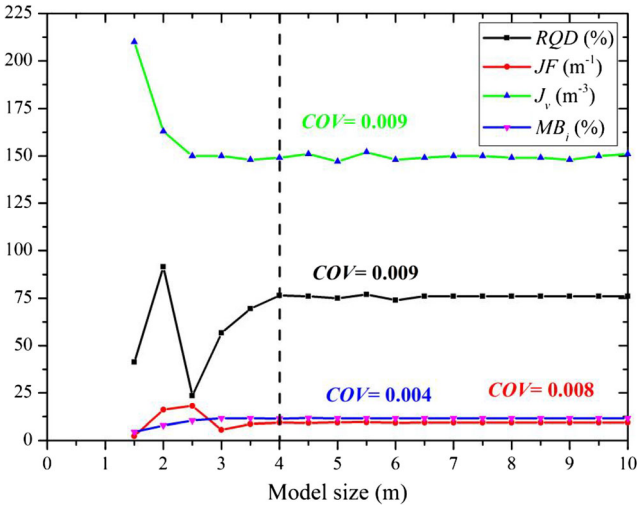

Fig. 2 REV determination for the *3DJN* model (*JP* = 0.5 m and *JS* = 0.13 m)

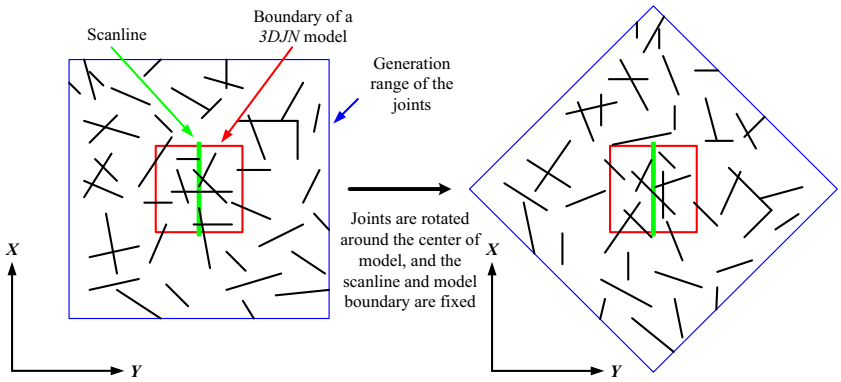

Fig. 3 A two-dimensional example to roughly illustrate the scanline setting in a model

block size: MB_i and V_b count blocks of all sizes in three dimensions, and RQD counts rock pieces greater than 100 mm in one dimension; however, JF and J_v quantify rock mass blockiness from the perspective of one- and three-dimensional joint density. In addition, although both MB_i and V_b are indirect measurements, their determination methods differ: V_b is estimated mainly by J_v, and MB_i is determined by certain techniques including three-dimensional joint network representation and rock block identification.

Compared to the RQD and JF, the MB_i index can take into account the joint persistence, because the three-dimensional block size corresponds well with various joint geometries (Kim et al. 2007). However, the RQD is controlled primarily by the one-dimensional joint density (their theoretical correlation is presented in Eq. (7), Section 3), which cannot capture the effect of joint persistence. Therefore, in the following sections, we attempt to replace the RQD and JF with MB_i in the RMR system in order to fully consider the rock mass jointing degree in three dimensions.

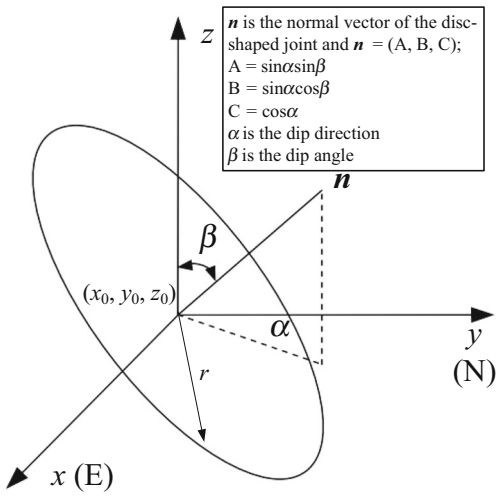

Fig. 4 Disc-shaped joint

Correlations of MB_i with RQD, JF and J_v

To consider all possible cases, multiple simulated experiments were conducted to obtain a large volume of artificial data sets.

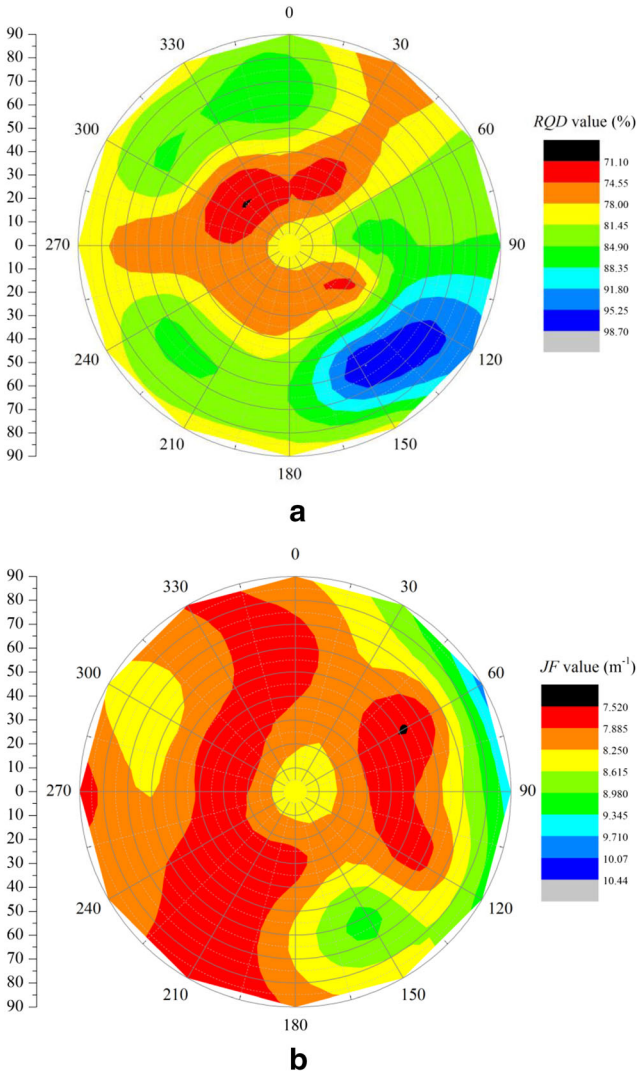

Fig. 5 RQD and JF values (in different directions) measured in a model. **a** RQD values and **b** JF values. The JS and JP values of the model are 0.17 m and 0.5 m, respectively

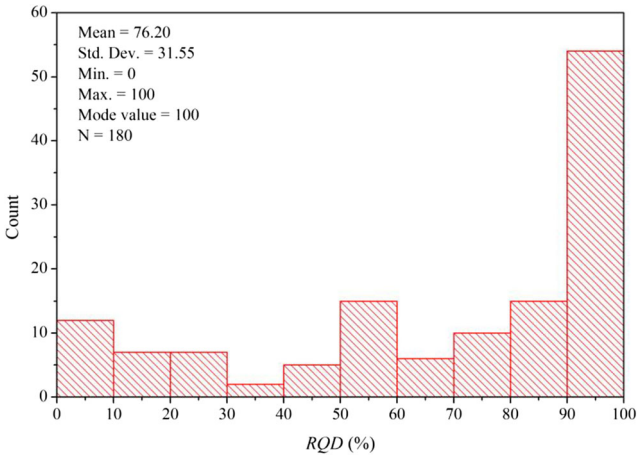

Fig. 6 Histogram of *RQD* (artificial data). *N* indicates the number of models

Under such ideal conditions, the correlations of MB_i with *RQD*, *JF* and J_v were evaluated. Validations are presented in Section 5, using a number of real data.

Design of simulated experiment

When the *JN* value is fixed, the joint density (or frequency, or spacing) has the greatest effect on the degree of rock mass jointing, followed by joint persistence (Bieniawski 1989; Shang et al. 2018), whereas the other joint geometrical parameters, such as joint orientation (*JO*) and distribution type, have negligible effects (Zhang et al. 2009). If all joint geometrical parameters are considered, the workload is too heavy. Therefore, the joint data in Xia et al. (2015) are employed (Table 3), including the average joint orientation, joint trace standard deviation and distribution type of joint traces. In this section, the joint parameters in Table 3 are fixed, and the *JS* and *JP* values are changed. In addition, *3DJN* models are constructed using the GeneralBlock program, and the block sizes are identified and recorded; these models are passed on to 3DEC, and a specific code is developed and executed in 3DEC, where *RQD*, *JF* and J_v values are determined.

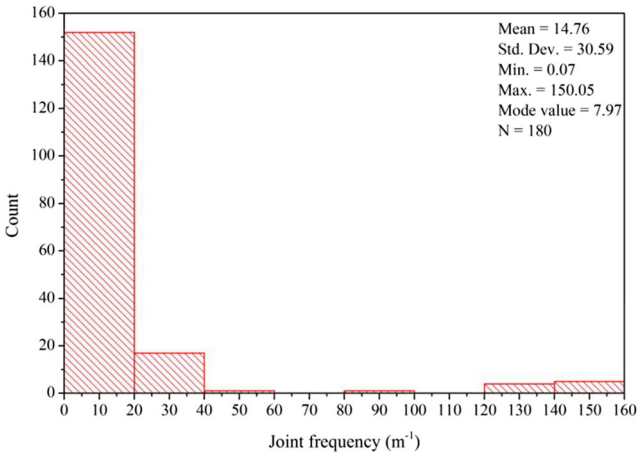

Fig. 7 Histogram of *JF* (artificial data)

Pairs of "*JS-JP*"

Since the degree of jointing is mainly affected by joint spacing (*JS*) and joint persistence (*JP*), the schemes of simulated experiments were developed by means of the following steps: (i) select a range of *JS* and *JP* values, and two groups of samples (i.e., *JS* and *JP*) can be obtained; and (ii) develop pairs of "*JS-JP*" by the cross joins of *JS* and *JP* values, respectively, from the two groups of samples, while other joint geometrical parameters remain fixed.

The joint spacing and persistence can be classified into seven and five intervals, respectively (ISRM 1978), as shown in Table 4. A total of 18 joint spacing values and 10 joint persistence values were selected, and two groups of samples (i.e., *JS* and *JP*) were obtained; therefore, 180 pairs of "*JS-JP*" were developed by the cross join method. It can be observed from Table 4 that most of the selected joint spacing values are in the range of 0.02 to 2 m, which reflects those commonly found in engineering practice (ISRM 1978; Bejari and Khademi Hamidi 2013; Riquelme et al. 2015; Buyer and Schubert 2017; Wong et al. 2018). The other joint geometrical parameters are fixed, as shown in Table 3. Based on these 180 pairs, 180 schemes are established, and 180 *3DJN* models with different structures are created. Some *3DJN* models (established using GeneralBlock) are presented in Fig. 1. It is noted that the distribution types of joint persistence values are in agreement with Table 3, and the joint spacing values are derived for three-dimensional joint densities (Xia et al. 2016):

$$d_3 = \frac{4}{\pi \times E\left(JP^2\right) \times JS} \tag{2}$$

where d_3 is three-dimensional joint density. This is because in many *3DJN* model generators, including GeneralBlock, the input parameters with regard to joint density are of three-dimensions.

The geometrical and mechanical properties are controlled predominantly by the size of the "sample" or "specimen" under investigation, i.e., the effect of the representative elementary volume (REV). Also, the geometrical REV is not the same as the mechanical REV, and geometrical and mechanical REV represent the geometrical and mechanical properties that have reached a

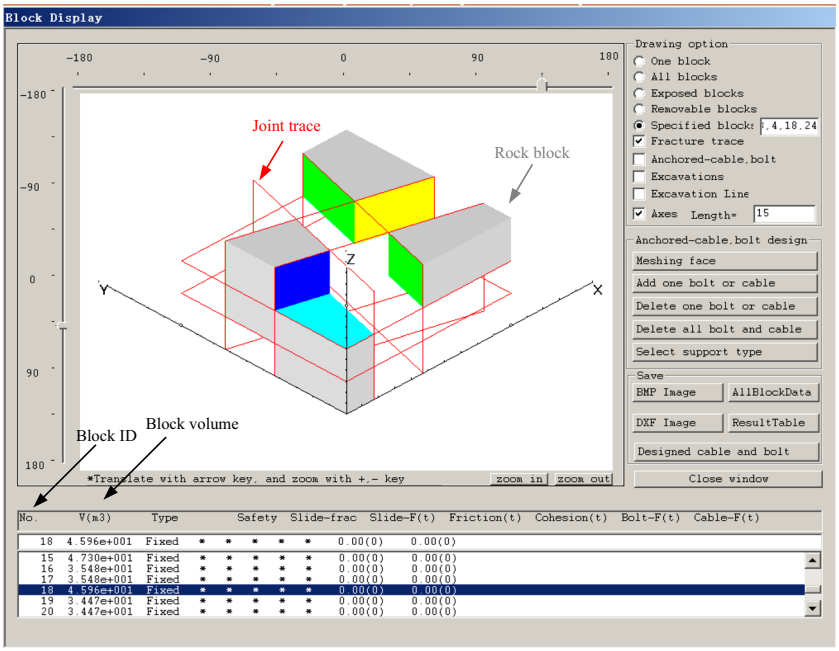

Fig. 8 An example to roughly illustrate the identification of block volume (this model (10 × 10 × 10 m) contains three joint sets which are orthometric)

constant behavior, respectively. In this study, all the parameters (e.g., *RQD*) are related to the structural and geometrical features of models. Thus, all of the *3DJN* models have met the size requirement for geometrical REV and are also greater than the joint persistence value. An example of REV determination is presented in Fig. 2. In this figure, the REV of a *3DJN* model (JP = 0.5 m and JS = 0.13 m), which is also shown in Fig. 1, was determined: when the model size is greater than 4 m, the coefficients of variation (*COV*) for *RQD*, *JF*, J_v and MB_i (the procedures for determining them are presented in Section 3.1.2) are all within the range of 0 to 0.5, and therefore the *REV* of this *3DJN* model is determined as 4 m. Additionally, in order to reasonably measure *RQD* values, the sizes of the *3DJN* models are all larger than 1.5 m.

Data acquisition

Data acquisition was carried out using 3DEC, with exception of the MB_i values. *RQD* and *JF* values were determined by setting scanlines in the *3DJN* models. To minimize the directional bias, the scanline and model boundary were fixed, and the joint network was rotated. In this way, the *RQD* and *JF* values in different directions could be measured, and the scanline length remained unaltered, as shown in Fig. 3. The scanline is perpendicular to ***XY*** plane (in a Cartesian coordinate system), and the intersection point is the model's center (0, 0, 0). Therefore, the scanline can be described as

$$\begin{cases} x_L = 0 \\ y_L = 0 \end{cases} \tag{3}$$

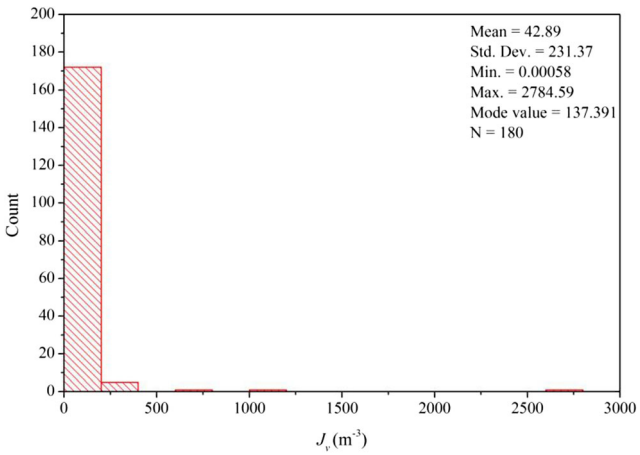

Fig. 9 Histogram of J_v (artificial data)

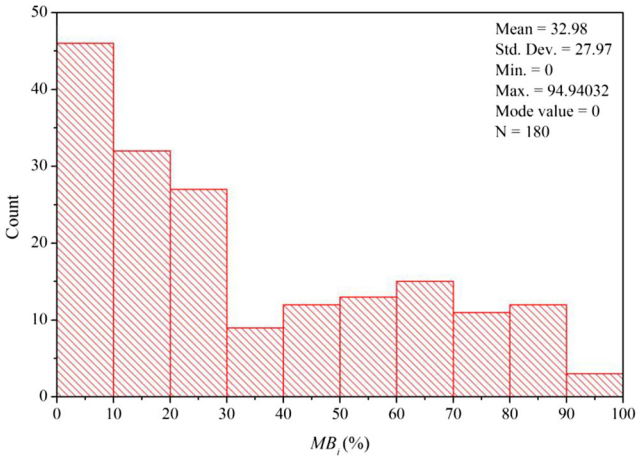

Fig. 10 Histogram of MB_i (artificial data)

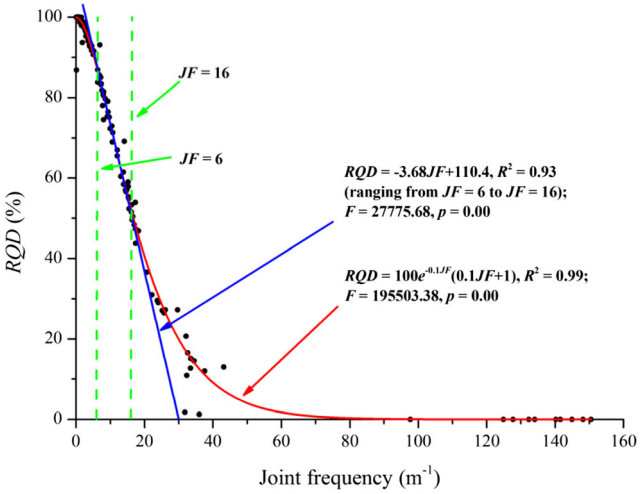

Fig. 11 Correlations between *RQD* and *JF* (artificial data)

The joint in a model (Fig. 4) can be represented as

$$\begin{cases} A(x-x_0)+B(y-y_0)+C(z-z_0)=0 \\ (x-x_0)^2+(y-y_0)^2+(z-z_0)^2=r^2 \end{cases} \quad (4)$$

where A, B and C are the components of a normal vector of a joint, respectively, x_0, y_0 and z_0 are the central coordinate values of a joint, and r is the joint radius. From Eqs. (3) and (4), an equation of the intersection of the joint and scanline can be established; if the solution of this equation is a real number, an intersection point exists between the joint and scanline, and vice versa. After the coordinates of the intersection points are obtained, the *RQD* and *JF* values can be easily calculated.

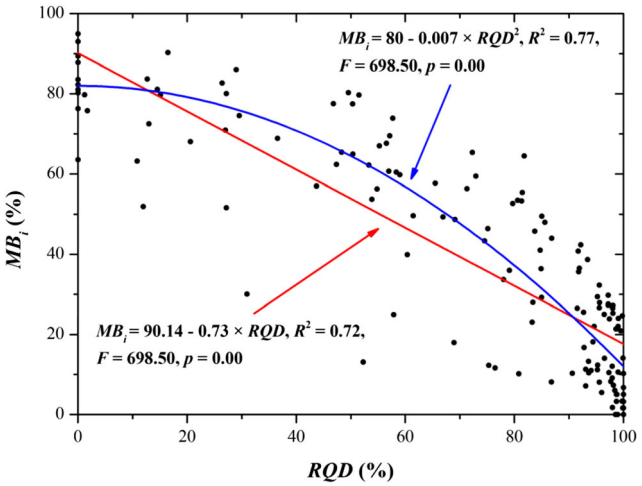

Fig. 12 Correlations between MB_i and *RQD* (artificial data). Note that the red and blue curves represent Eqs. (9) and (10), respectively

The rotation of a joint network can be achieved by the rotation matrix $\boldsymbol{A}$ (Zheng et al. 2014):

$$\boldsymbol{A}=\begin{bmatrix} cos\beta_1 \bullet cos\alpha_1 & -\sin\alpha_1 & \sin\beta_1 \bullet cos\alpha_1 \\ cos\beta_1 \bullet \sin\alpha_1 & cos\alpha_1 & \sin\beta_1 \bullet \sin\alpha_1 \\ -\sin\beta_1 & 0 & \cos\beta_1 \end{bmatrix} \quad (5)$$

where α_1 is the rotation angle of the joint network in the dip direction, and β_1 is the rotation angle of the joint network in the dip angle. Therefore, the joint central coordinates after rotation (x', y', z') can be obtained by

$$\begin{bmatrix} x' \\ y' \\ z' \end{bmatrix} = \boldsymbol{A} \bullet \begin{bmatrix} x_0 \\ y_0 \\ z_0 \end{bmatrix} \quad (6)$$

Additionally, joint orientation will also change after the rotation of the joint network. Similarly, the joint orientation after rotation can be calculated using $\boldsymbol{A}$; the detailed processes are not repeated in this section.

Overall, a large number of *RQD* and *JF* values can be determined from a *3DJN* model (an example is shown in Fig. 5), and their averages are defined as unique representative *RQD* and *JF* values. The means and standard deviations of the *RQD* and *JF* values for all *3DJN* models are shown in Figs. 6 and 7. The two figures indicate that the *RQD* values fall mainly within the interval of 90–100, and the *JF* values fall mainly within the interval of 0–20.

Other unsettled questions involve the determination of J_v and MB_i. In fieldwork, the J_v is often measured by the average spacing for well-defined joint sets (Palmstrom 2005), but obviously, this approach is inapplicable in this study, because it leads to identical results produced by various *3DJN* models. With regard to the essence of the J_v concept, i.e., the number of joints per unit volume of rock mass, the J_v is found to be equivalent to the P30 (fracture/m^3) (Dershowitz et al. 2003). In this work, the P30 values for all *3DJN* models were determined using the built-in codes in 3DEC. Additionally, the sizes of blocks inside the *3DJN* models were identified using GeneralBlock, as shown in Fig. 8, and the MB_i values were determined according to Eq. (1). The J_v and MB_i values for all *3DJN* models are shown in Figs. 9 and 10. It can be seen that the J_v values fall mainly in the interval of 0–200, and the standard deviation is very large (231.37), because several *3DJN* models contain very small and dense joints. For example, the J_v of the *3DJN* model ($JP = 0.5$ m and $JS = 0.01$ m) is 2784.59. The MB_i values fall mainly within the interval of 0–30.

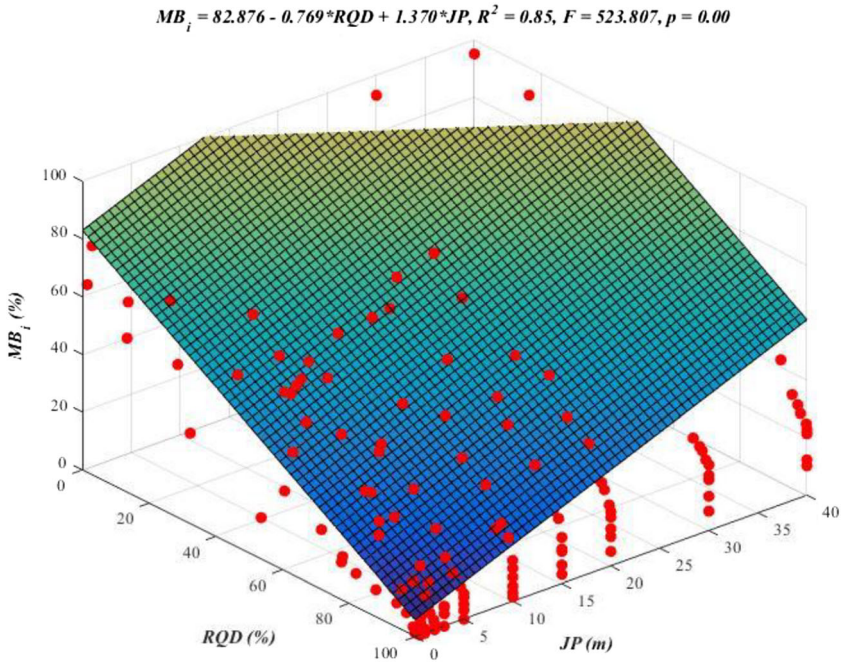

Fig. 13 Correlation between MB_i and RQD and JP (artificial data), corresponding to Eq. (11)

Validating the effectiveness of artificial data

In Section 3.1, 180 *3DJN* models were established, and a substantial amount of artificial data was obtained. Before assessing the correlations between MB_i and $RQD/JF/J_v$, it is necessary to check the validity of the artificial data, i.e., whether these artificial data reflect the objective trend.

The relation between RQD and JF (Priest and Hudson 1976) is

$$RQD = 100e^{-0.1JF}(0.1JF + 1) \tag{7}$$

For the JF values ranging from 6 to 16, the linear relation between RQD and JF is

$$RQD = -3.68JF + 110.4 \tag{8}$$

Therefore, a scatter plot of artificial RQD and JF values was created, and regression analysis was carried out, which is presented in Fig. 11. The figure shows that the data points are fitted using Eqs. (7) and (8), and the coefficients of determination are 0.99 and 0.93, respectively. Additionally, F tests were carried

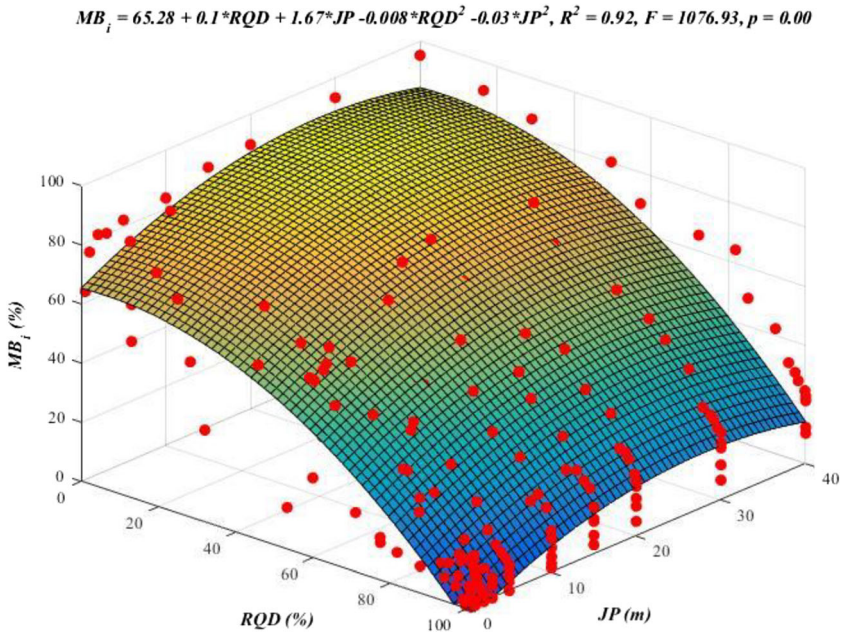

Fig. 14 Correlation between MB_i and RQD and JP (artificial data), corresponding to Eq. (12)

Table 5 Collinearity statistics of Eq. (11)

Independent variables	Unstandardized coefficients		Standardized coefficients	t	Significance	Variance inflation factor (VIF)
	B	Std. Error	Beta			
Constant	82.876	2.237		37.054	0.00	
RQD	−0.769	0.025	−0.867	−30.336	0.00	1.00
JP	1.370	0.124	0.316	11.056	0.00	1.00

out, and the F and p values suggested that the null hypotheses were rejected, and that the two regression models, i.e., Eqs. (7) and (8), were significant. This means that the results of the simulation experiment are effective and reliable, and moreover that the artificial data sets produced by the theoretical *3DJN* models are in line with the objective trends.

Correlation between MB_i and *RQD*

In the field of rock mechanics and rock engineering, *RQD* has received much attention over the past few decades. It was found that *RQD* is closely related to *JF*, J_v, P-wave velocity, deformation modulus and unconfined compressive strength (Feng and Jimenez 2015; Zhang 2016). Since the MB_i is a direct representation of block size, similar to *RQD*, the MB_i may correlate well with the *RQD*.

Based on Figs. 6 and 10, a scatter plot of MB_i and *RQD* was created (note that some data points were deleted because too many *RQD* values were close to 100%, which can lead to invalid curve-fitting). Linear and nonlinear regression analyses were conducted (Fig. 12), which yielded

$$MB_i = 90.14 - 0.73 \times RQD \tag{9}$$

$$MB_i = 80 - 0.007 \times RQD^2 \tag{10}$$

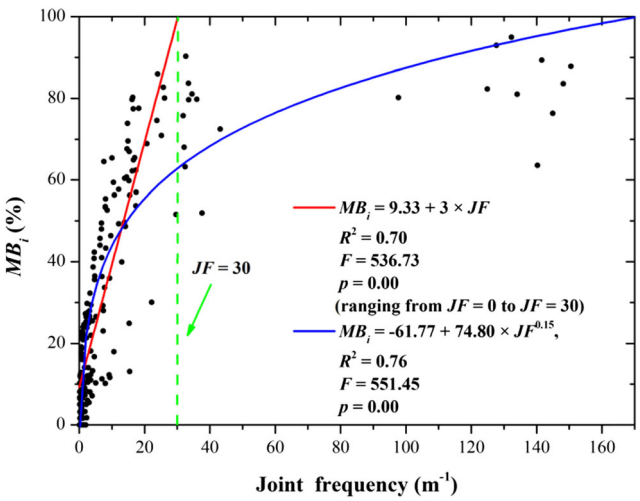

Fig. 15 Correlations between MB_i and *JF* (artificial data), corresponding to Eqs. (13) and (14)

Figure 12 shows that the two coefficients of determination are 0.72 and 0.77, respectively, and the F and p values indicate than the null hypotheses are rejected and the regression models are significant.

Considering that the block sizes are controlled mainly by joint spacing and joint persistence (Kim et al. 2007), and that the *RQD* concept takes into account only the core pieces longer than 100 mm, joint persistence was involved in the assessment of the correlation between MB_i and *RQD*. Therefore, multiple linear and nonlinear regression analyses were performed (Figs. 13 and 14), which yielded

$$MB_i = 82.876 - 0.769 \times RQD + 1.370 \times JP \tag{11}$$

$$MB_i = 65.28 + 0.1 \times RQD + 1.67 \times JP - 0.008 \times RQD^2 - 0.03 \times JP^2 \tag{12}$$

Figures 13 and 14 show that the coefficients of determination are 0.85 and 0.92, respectively, and the F and p values indicate that the null hypotheses are rejected and the two regression models are significant. Additionally, Eq. (11) is a multiple linear model, and hence, the collinearity statistics was carried out, which is presented in Table 5. A review of Table 5 indicates that all VIF values for each variable are less than 10, indicating that no strong correlation exists between the two independent parameters.

From Eqs. (9)–(12), four inverse relations between MB_i and *RQD* were found, namely, the larger the MB_i, the smaller the *RQD*. Figure 12 also shows that when the *RQD* is 0, the MB_i values vary from 60 to 100; when the *RQD* is 100, the range of MB_i values is approximately 0–30. This may be attributed to the conceptual difference between MB_i and *RQD*, i.e., (i) the *RQD* counts only the core pieces longer than 100 mm, while the MB_i consider all blocks; and (ii) joint persistence is neglected with the *RQD* method.

Correlation between MB_i and *JF*

Based on Figs. 7 and 10, the MB_i values were plotted with *JF*, as shown in Fig. 15. The nonlinear regression analysis yields

$$MB_i = -61.77 + 74.80 \times JF^{0.15} \tag{13}$$

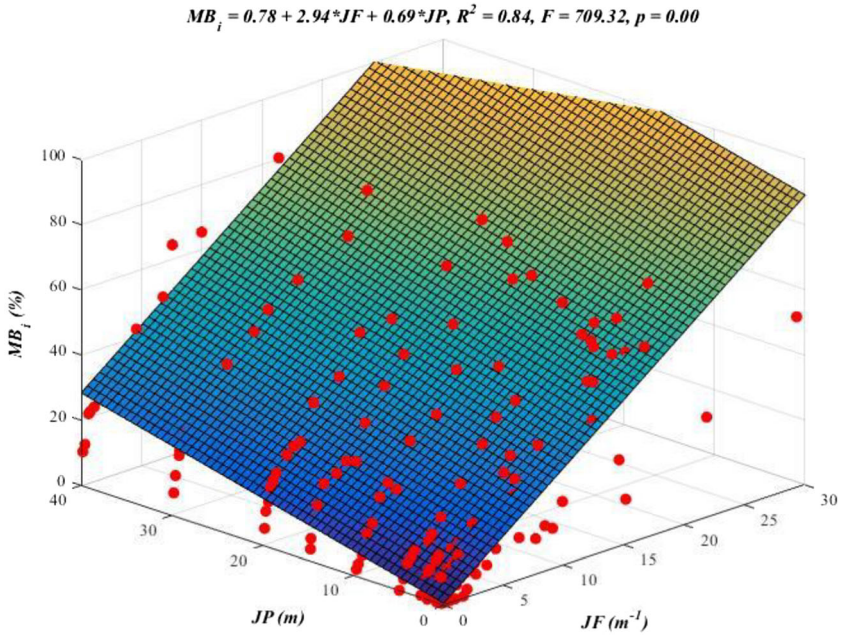

Fig. 16 Correlations between MB_i and JF (artificial data), corresponding to Eq. (15)

The coefficient of determination is 0.76, and the F and p-values are 551.45 and 0.00, respectively, which suggests that the null hypothesis is rejected, and the regression model is significant. For JF values less than 30, a linear relation is found

$$MB_i = 9.33 + 3 \times JF \tag{14}$$

The coefficient of determination is 0.70, and the F and p-values are 536.73 and 0.00, respectively. Additionally, when the JF is greater than 30, the MB_i shows a poor relation with JF.

By incorporating the JP into the assessment, multiple linear and nonlinear analyses were conducted (Figs. 16 and 17), which yielded

$$MB_i = 0.78 + 2.94 \times JF + 0.69 \times JP \tag{15}$$

$$MB_i = -8.09 + 5.18 \times JF + 1.69 \times JP - 0.11 \times JF^2 - 0.03 \times JP^2 \tag{16}$$

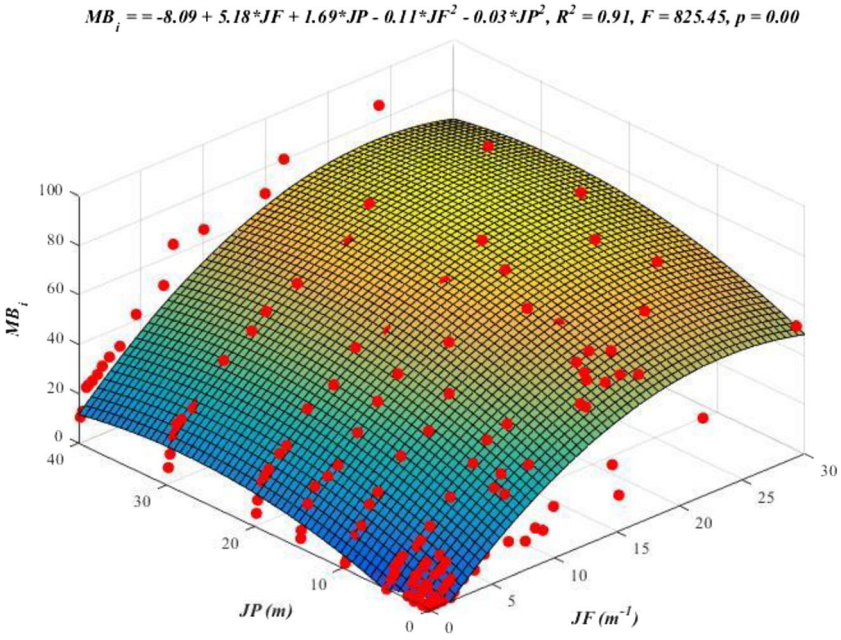

Fig. 17 Correlations between MB_i and JF (artificial data), corresponding to Eq. (16)

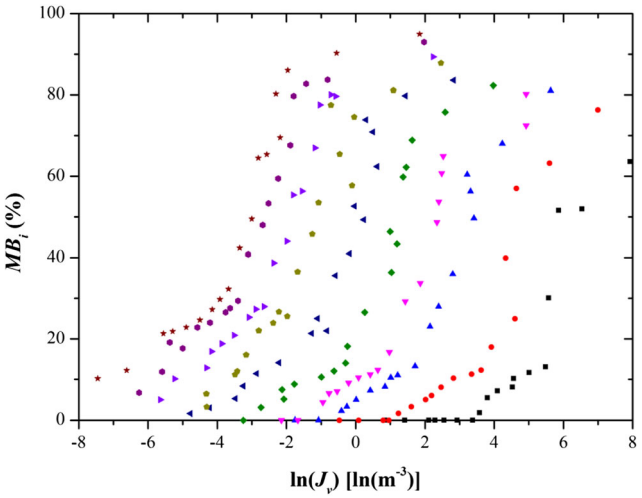

Fig. 18 Scatter plot of MB_i and J_v (artificial data)

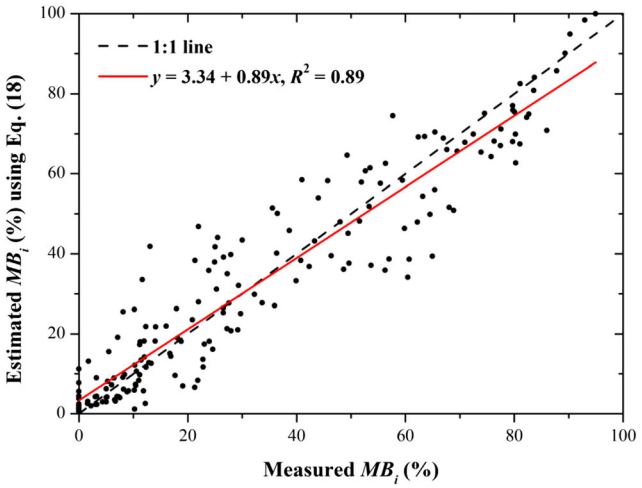

Fig. 20 Comparison between measured MB_i values (artificial data) and estimated MB_i values using Eq. (17)

The corresponding coefficients of determination are 0.84 and 0.91. F tests were carried out, and the F and p values indicate that the null hypotheses were rejected, and the regression models are significant.

Correlation between MB_i and J_v

Based on Figs. 9 and 10, the scatter plot of MB_i vs. J_v is delineated in Fig. 18. Note that the difference in orders of magnitude between various J_v values is too large, so the $\ln(J_v)$ is employed, and the data points with different colors denote various joint persistence. It is observed from Fig. 18 that the data points are very discrete, for which regression analysis cannot be properly performed; however, when the color (i.e., the joint persistence) is identical, the MB_i values increase with the increase in J_v. Therefore, it is better to take into consideration the joint persistence.

Multiple nonlinear regression analysis (Fig. 19) yields

$$MB_i = \frac{74.383 + 0.864 \times JP}{1 + e^{-2.489+8.06\times0.842^{JP}-0.938\times\ln(J_v)}} \tag{17}$$

Additionally, the coefficient of determination is 0.89, and the F and p values are 603.96 and 0.00, respectively, suggesting that the null hypothesis is rejected, and the regression model is significant.

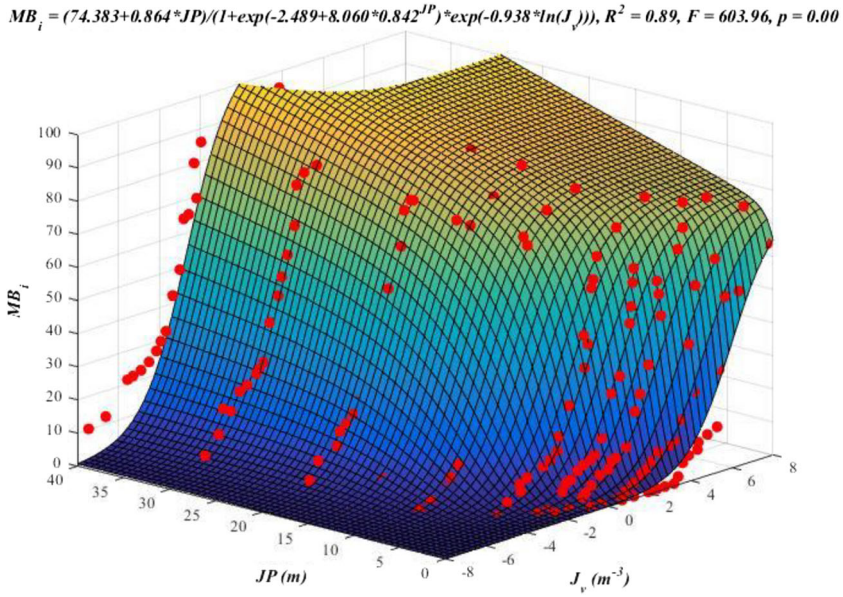

Fig. 19 Correlations between MB_i and J_v (artificial data), corresponding to Eq. (17)

Table 6 Determination of R_M

Jointing/ blockiness degree	Integrated/ non-blockiness	Relatively integrated/slight blockiness	Poorly integrated/ moderate blockiness	Relatively fractured/ blockiness	Fractured/ serious blockiness
MB_i	0–7%	7–27%	27–55%	55–85%	85–100%
R_M	37–40	29–37	18–29	6–18	0–6

A comparison between measured MB_i values and estimated values was performed using Eq. (17), which is presented in Fig. 20. Although the coefficient of determination is rather high, the fitted curve is below the 1:1 line, meaning that the measured values are greater than the estimated values.

RMR_{mbi} and its preliminary validation

Development of RMR_{mbi}

Inaccurate measurements of block size may lead to unreliable rock mass classification results (Palmstrom 2005; Aydan et al. 2014). The combined use of *RQD* and *JF* in the *RMR* system is limited, because (i) both *RQD* and *JF* values are orientation-dependent; (ii) the *RQD* method counts only core pieces greater than 100 mm, which is sometimes unreasonable (Harrison 1999); (iii) both the *RQD* and *JF* methods neglect joint persistence; and (iv) the ratings of *RQD* plus *JF* are a repetition of joint density, resulting in the doubling of the influence of joint density on the final *RMR* rating. Although some researchers (Koutsoftas 2017) have maintained that these limitations would not reduce the applicability of the *RMR* system, these theoretical limitations do exist in reality, and thus improvement of the subsystem (i.e., the ratings of *RQD* plus *JF*) of the *RMR* is desired.

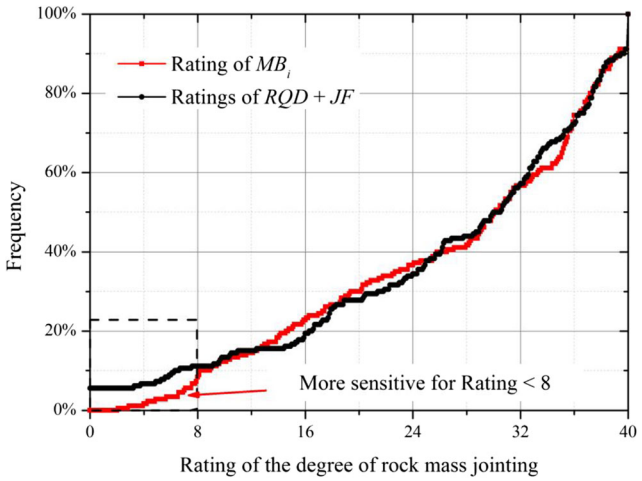

Fig. 22 Comparison of R_M and R_{RQD+JF} based on the cumulative frequency curves (artificial data)

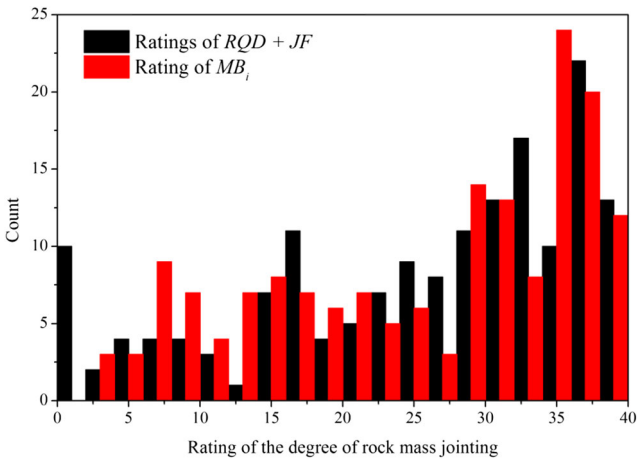

Fig. 21 Histograms of R_M and R_{RQD+JF} (artificial data)

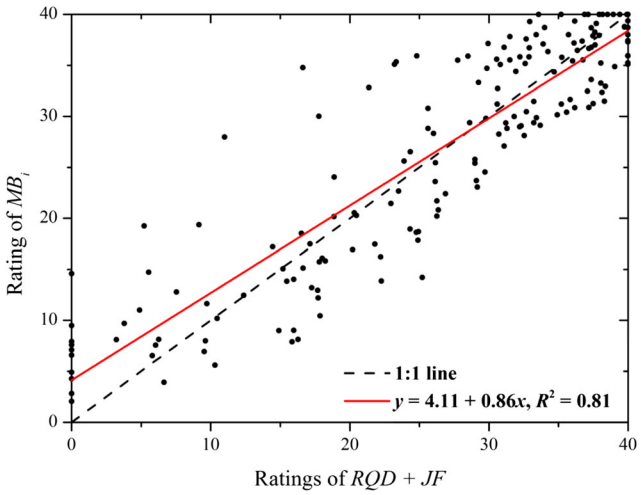

Fig. 23 Comparison between R_M and R_{RQD+JF} based on the 1:1 line (artificial data)

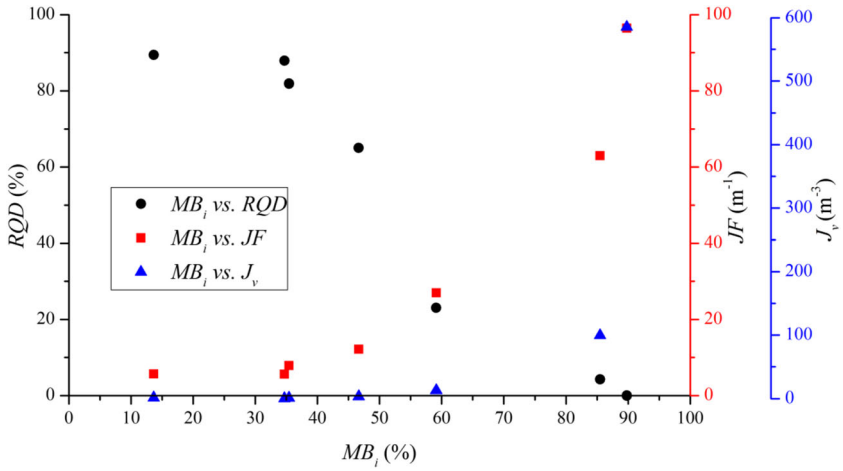

Fig. 24 MB_i, RQD, JF and J_v values acquired from real cases

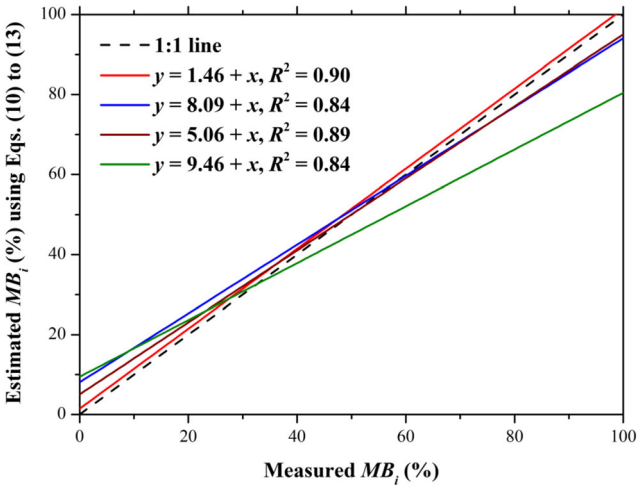

Fig. 25 Comparison of the four regression models, i.e., Eqs. (9)–(12) (real cases). Note that in the legend, the red, blue, brown and green straight lines are the fitted curves of the measured MB_i values (real cases) and the estimated MB_i values using Eqs. (9)–(12), respectively

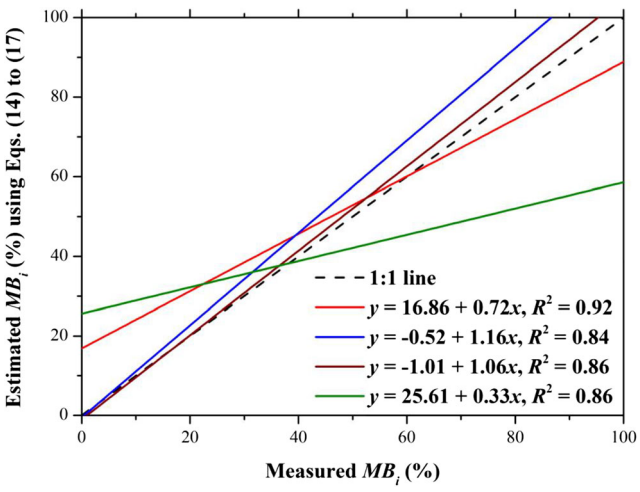

Fig. 26 Comparison of the four regression models, i.e., Eqs. (13)–(16) (real cases). Note that in the legend, the red, blue, brown and green straight lines are the fitted curves of the measured MB_i values (real cases) and estimated MB_i values using Eqs. (13)–(16), respectively

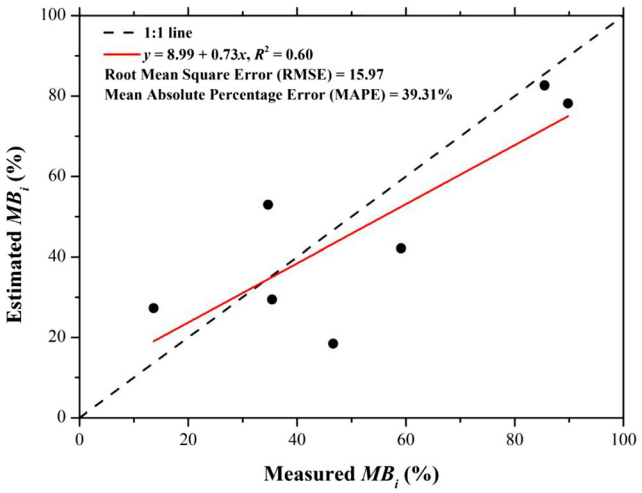

Fig. 27 Comparison of measured MB_i values (real cases) and estimated MB_i values using Eq. (17)

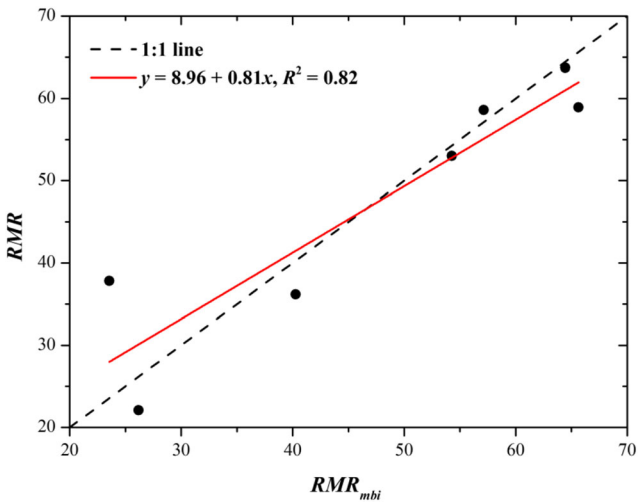

Fig. 28 Comparison between RMR_{mbi} and RMR based on real cases

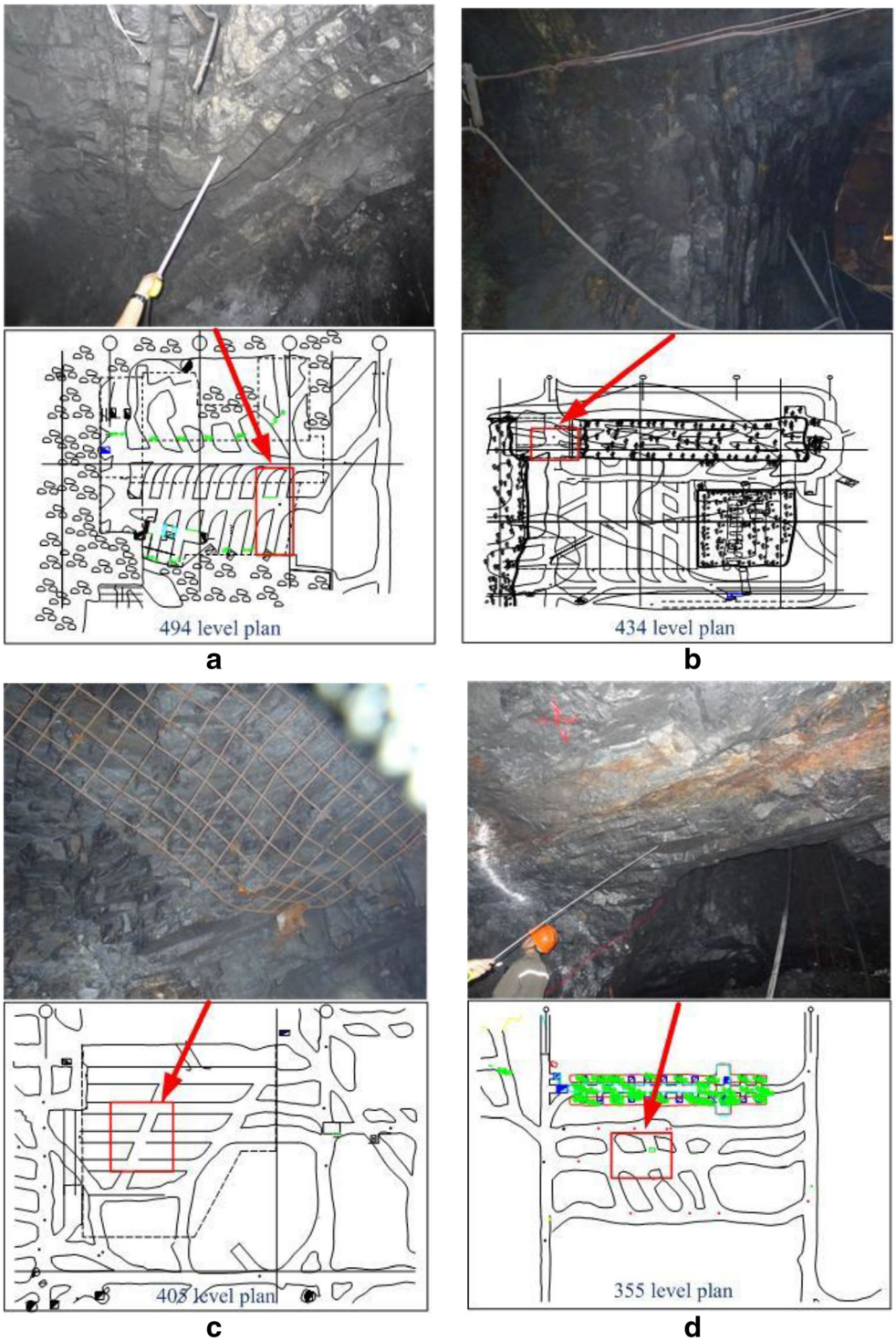

Fig. 29 Locations and ground conditions of the four study sites. **a** Study site 1; **b** study site 2; **c** study site 3; and **d** study site 4

Motivated by the need to improve the *RMR* system, an attempt was made to substitute the combined use of *RQD* and *JF* with MB_i, while keeping the other input parameters unchanged; this version is referred to as RMR_{mbi}. As shown in Sections 2 and 3, the main advantages of using MB_i to replace *RQD* and *JF* are as follows: (i) the MB_i is a three-dimensional measurement and is not orientation-dependent; (ii) the MB_i counts blocks of all sizes; (iii) joint persistence is considered, as shown in Section 3; and (iv) the MB_i does not repeatedly calculate the joint density. The rating of MB_i (R_M) can be determined using a continuous function, as described by Eq. (18).

$$R_M = 40–0.4 \times MB_i \tag{18}$$

Fig. 30 Field investigation. **a** Joint mapping and **b** core drilling

The greater the value of the MB_i, the smaller the degree of rock mass jointing, and the poorer the rock mass quality, and vice versa. Table 6 can be used to determine the R_M value. Therefore, R_M is inversely proportional to MB_i. The other input parameters, including, intact rock uniaxial compressive strength, are kept unchanged.

Preliminary validation of the viability of RMR_{mbi}

Since the RMR_{mbi} and traditional RMR systems are different from the characterization of rock mass structure, only the R_M and R_{RQD+JF} were compared. R_{RQD+JF} (Warren et al. 2016) can be calculated by

$$R_{RQD} = 0.2 \times \mathrm{RQD} \tag{19}$$

$$R_{JF} = -3.767 \times \ln(JF) + 16.482 \tag{20}$$

Therefore, $R_{RQD+JF} = R_{RQD} + R_{JF}$.

Actually, the application of RMR_{mbi} in real cases is inadequate, because it is a new modification with regard to RMR. To confirm its viability, the results of simulated experiments considering many circumstances were used. The R_M and R_{RQD+JF} were applied to the artificial data sets (Figs. 6, 7 and 10), and the results are presented in Fig. 21, which shows that most of the R_M and R_{RQD+JF} values fall within the interval 30–40. The cumulative frequency curves are delineated in Fig. 22. The figure shows that for the interval of 8–40, the two curves are very smooth and have extremely similar trends, meaning that the two subsystems (i.e., R_M and R_{RQD+JF}) share an ability to distinguish the rock masses of various structures.

Figure 22 also indicates that for the interval of 0–8, the R_{RQD+JF} shows poor "performance", because the cumulative frequency curve of R_{RQD+JF} does not start from the origin; however, in this interval, the curve of R_M grows from the origin and shows a more natural transition, which means that the R_M is more sensitive to rock masses with a high degree of jointing and can properly distinguish them. If one classification system is able to differentiate objects with a greater degree of refinement than another system, then it can be said that this system is better (Warren et al. 2016). Therefore, the R_M is viable.

The correlation between R_M and R_{RQD+JF} values was evaluated based on the 1:1 line, which is presented in Fig. 23. It is found that although the MB_i can be treated as an extension of RQD, the R_M and R_{RQD+JF} yield slightly different results. As shown in Fig. 23, when the R_{RQD+JF} is close to 0, the R_M values vary from 0 to 15; when the R_{RQD+JF} is near 40, the R_M values vary in the range of 35–40. However, the best-fitted curve is very close to the 1:1 line, with a rather high coefficient of determination.

Additionally, for the RQD and JF values determined in the simulated experiments, the directional bias has been the removed (i.e., they properly reflect the degrees of rock mass jointing), but in fieldwork, it is very difficult to guarantee that the RQD and JF values will not be biased by direction. This is why the substitution was performed. This problem is completely overcome in the RMR_{mbi} system, which is a particular advantage of this RMR_{mbi}.

Validations based on actual data

Validating the correlations of MB_i with RQD, JF and J_v based on actual data

Validation studies were performed based on real case histories (Guangxi University and Huaxi Group 2013; Central South University et al. 2011; Wang 2011; Pan 2012). The MB_i values were plotted with the RQD, JF

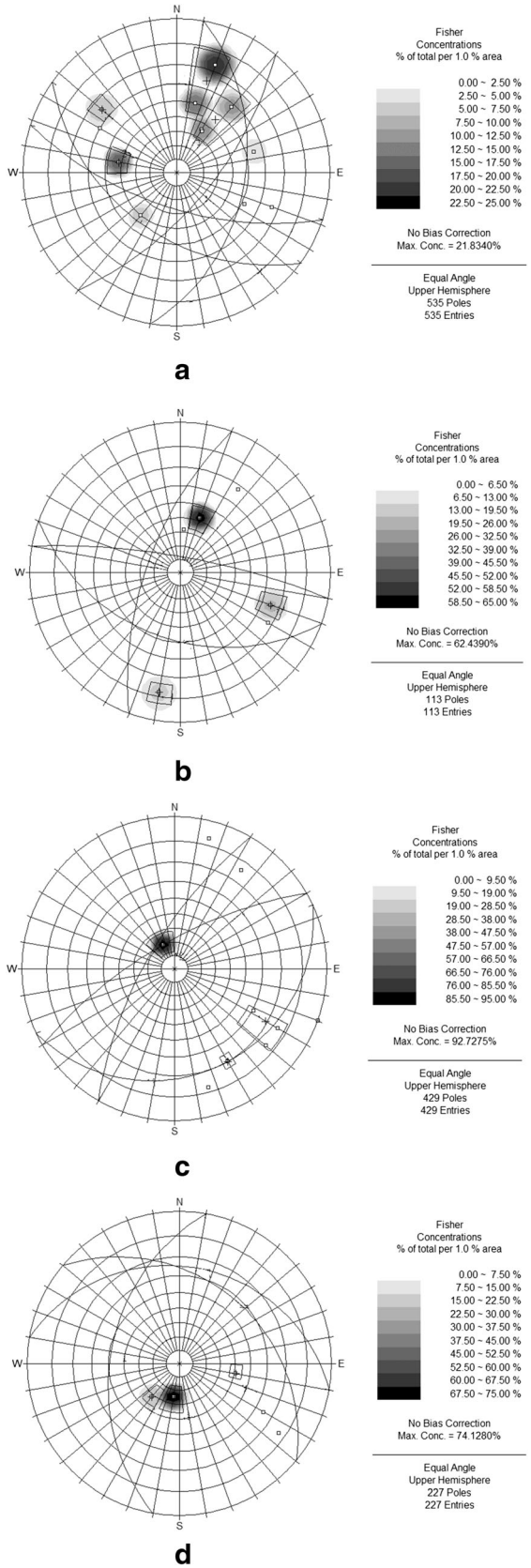

Fig. 31 Contour plots of joint poles collected from the four study sites. **a** Study site 1; **b** study site 2; **c** study site 3; and **d** study site 4

and J_v values in Fig. 24. Based on these real data (Fig. 24), the assessed correlations (i.e., Eqs. (9)–(17)) were verified:

(i) The fitting analyses were applied to the actual MB_i values and estimated MB_i values using Eqs. (9)–(12), and the fitted curves are presented in Fig. 25. The figure shows that all fitted curves are very close to the 1:1 line, indicating that the four correlation equations (i.e., Eqs. (9)–(12)) properly reflect the relationship of MB_i and RQD. Considering the coefficients of determination and the proximity degree of the 1:1 line and fitted curves, it can be concluded that Eq. (9) estimates the MB_i value more accurately.

(ii) According to the actual JF values presented in Fig. 24, the estimated MB_i values were produced using Eqs. (13)–(16). Fitting analyses were carried out based on the actual MB_i values and estimated MB_i values by JF, which are illustrated in Fig. 26. It can be seen from Fig. 26 that almost all the actual MB_i values are less than the estimated values. Additionally, the coefficient of determination of the red curve is larger, but the associated curve is far from the 1:1 line; the blue and brown curves are closer to the 1:1 line, with lower coefficients of determination. Considering the coefficients of determination and the proximity degree of the 1:1 line and fitted curves, it can be concluded that Eq. (15) estimates the MB_i value more accurately.

(iii) From Eq. (17), the estimated MB_i values were obtained by the J_v values (Fig. 24). Fitting analysis was performed, and the fitted curve is presented in Fig. 27. It is observed that the fitted curve is very close to the 1:1 line, with a coefficient of determination of 0.60, which is not very high. Also, the mean absolute percentage error (MAPE) and root-mean-square error (RMSE) of the measured and estimated values are 39.31% and 15.97, respectively. The lower coefficient of determination and larger errors can be explained by the relatively weak reliability of Eq. (17) or the lack of enough real data.

Figures 25, 26 and 27 show that none of the fitted curves are too far away from the 1:1 line, and in fact, some curves are very close to the line. Moreover, the corresponding coefficients of determination are rather high, with the smallest being 0.60. It can be concluded that the correlations of MB_i with RQD, JF and J_v, which were obtained from the artificial data sets, are capable of being applied to the real data and are extremely sound.

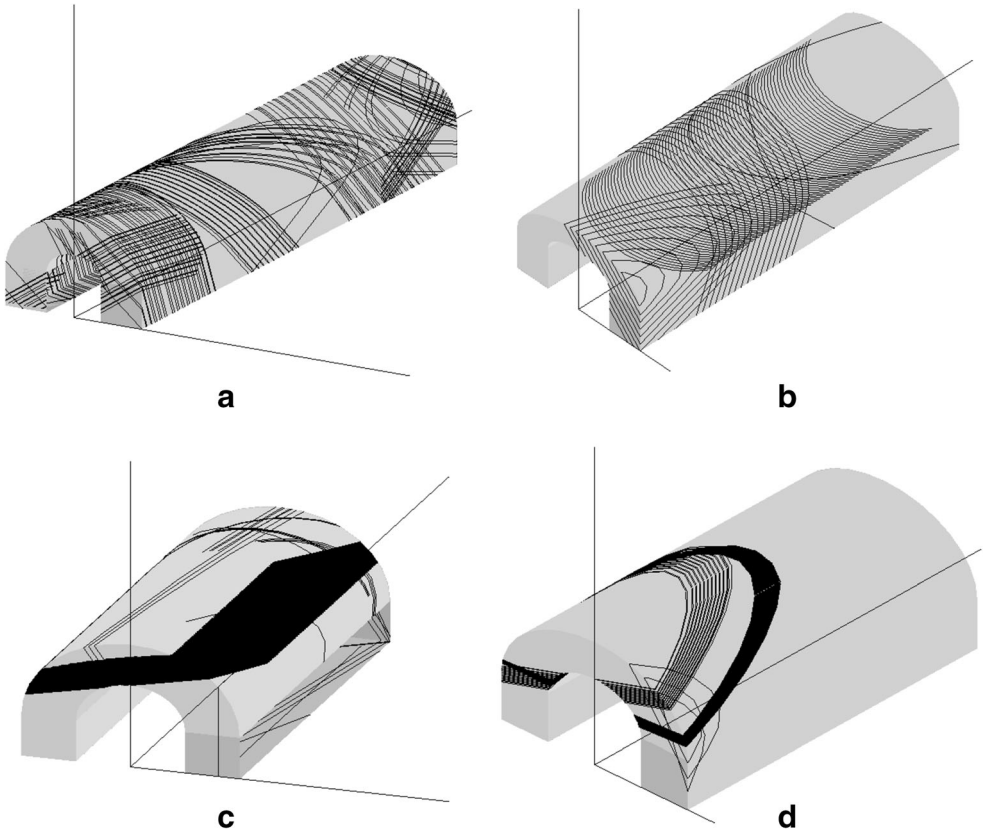

Fig. 32 Joint network models of the four sites. **a** Study site 1 (with drift length of 20 m and height of 2.8 m); **b** study site 2 (with drift length of 10 m and height of 3.2 m); **c** study site 3 (with drift length of 10 m and height of 3.2 m); and **d** study site 4 (with drift length of 10 m and height of 3.2 m). Note that only the large-scale joints are exhibited, and the small-scale joints are unobservable

Application of RMR_{mbi} and its comparison with RMR

Comparative analysis of RMR_{mbi} and RMR

In Section 4, the viability of RMR_{mbi} was preliminarily verified based on the artificial data sets, which confirm that the ability of RMR_{mbi} to differentiate rock masses with various structures is better than that of RMR (Fig. 22). In this section, the real data values (presented in Fig. 24) and the other input parameters (i.e., intact rock uniaxial compressive strength, joint condition and groundwater condition) are used to determine the final RMR_{mbi} and RMR values, and a comparison between RMR_{mbi} and RMR is subsequently carried out, as shown in Fig. 28. As seen in Fig. 28, the fitted curve is fairly close to the 1:1 line, suggesting that in some cases they have similar a ability to differentiate the rock mass quality.

Figure 28 shows few data, which means that at times, RMR_{mbi} is the same as RMR. Actually, because the real application of RMR_{mbi} is inadequate, simulated experiments were conducted in this study. Figure 22 indicates that R_M is better from the perspective of assessing rock mass structures with a rating of < 8 (Section 4.2). Therefore, the R_M and RMR_{mbi} are viable, because RMR_{mbi} is just different from RMR in evaluating rock mass jointing degree.

Some typical case studies of RMR_{mbi}

The Tongkeng Mine project was launched by a subsidiary corporation of the Huaxi Group Co., Ltd., Guangxi, China, which is owned by the Chinese government, and has a yearly capacity of 2 million tons or more. Three large ore bodies occur in this mine, i.e., Ximaidai, and no. 91 and 92 ore bodies. The exploitation of ore body no. 91 has been completed, and ore body no. 92 is under production, with probable mineral reserves of 30 million tons.

The no. 92 ore body occurs in silicalite and limestone, and is a large, thick ore body with a gentle dip angle. The minerals vary, and mainly include cassiterite, pyrite, marmatite, pyrrhotite and arsenopyrite, and quartz is the typical gangue mineral. When the caving method is used, instabilities (e.g., ground fall, sidewall spalling and roof collapse) frequently appear due to the incipient joint swarm, high ground stress and blasting disturbance, and some installed supports always fail.

Four study sites were selected in which to perform rock mass quality classification. Study site 1 is in the T214 stope at the 494 level, which is the intersection between the no. 14 production drift and ventilation gallery; study site 2 is in the T201 panel at the 434 level; study site 3 is in the no. 2 panel at the 405 level, whose center is the intersection between the no. 3 drill access and ventilation drift; and study site 4 is in the undercut chamber at the 355 level. The locations and ground

Table 7 RMR_{mbi} and RMR values for the four study sites

Site no.	Uniaxial compressive strength of intact rock (MPa)/score	RQD (%)/score	Joint frequency (m^{-1})/score	MB_i (%)/score	Fracture condition/score	Ground water/Score	Rating adjustment for joint orientation (mines)/ score	R_{RQD+JF}	R_M	RMR	RMR_{mbi}
1	81/6.08	28.7/5.74	11.49/7.28	62.25/15.1	Slickenside facture surface, separation = 1 mm, and medium continuous/10	Completely dry/15	−4	13.02	15.1	40.10 (III)	42.18 (III)
2	82/6.15	69.5/13.9	6.67/9.34	74.9/10.04	Slightly rough surface, separation <1 mm, and low continuous/20	Damp/10	−10	23.24	10.04	49.39 (III)	36.19 (IV)
3	85/6.38	40.6/8.12	6.67/9.34	92.04/3.18	Smooth fracture surface, separation <5 mm, and medium continuous/10	Dripping/4	−5	17.46	3.18	32.83 (IV)	18.56 (V)
4	79/5.93	28.6/5.72	17.54/5.69	16.3/33.48	Slightly rough surface, separation <1 mm, and low continuous /20	Wet/7	−2	11.41	33.48	42.34 (III)	64.41 (II)

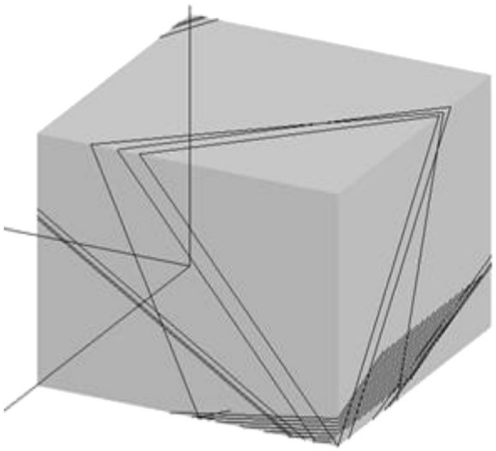

Fig. 33 Sub-joint network model of the study site 4 (5 m × 5 m × 5 m)

conditions of these sites are illustrated in Fig. 29. Additionally, joint mapping and core drilling were carried out, which is shown in Fig. 30. The joint orientation data are presented in Fig. 31.

Based on the joint information collected, the joint network models of the four study sites were established, and are shown in Fig. 32. The values of all input parameters of RMR_{mbi} and RMR were measured, and the projected features were also considered, as shown in Table 7. In addition, the MB_i values were calculated by identifying the blocks inside the cubic sub-joint network models to arrive at the REV sizes (Fig. 33), which are extracted from the models presented in Fig. 32.

Table 7 shows that with exception of study site 1, the RMR_{mbi} and RMR ratings are divergent. To compare the two systems, the field situations are presented in Table 5. The rock mass classes by stand-up span time are shown in Table 9. From Tables 7, 8 and 9, it can be observed that the RMR_{mbi} is more reliable; for example, for study site 3, the RMR rating is IV, and in Table 9, the rock mass stand-up time is expected to be approximately 10 h for a span of 2.5 m. However, with respect to the field situation, when the gallery is formed, a large-scale collapse occurs immediately; very long and dense rock bolts are systematically installed, with wire mesh and shotcrete of high thickness. Obviously, the RMR_{mbi} rating (V) is more reasonable. In short, therefore, based on the field situation, the following can be concluded: for study site 1, both the RMR_{mbi} and RMR ratings are rational; for study sites 2 and 3, the RMR ratings are overestimated, because the field situations are worse, and the expected stand-up time derived by RMR_{mbi} ratings are in keeping with the actual conditions. For study site 4, the RMR rating is conservative, and the RMR_{mbi} rating is appropriate.

A review of Table 7 also shows that the discrepancy between the R_{RQD+JF} and R_M values for the study sites (aside from study site 1) are very significant. Palmstrom (2005) found that when one-dimensional measurements of rock mass jointing degree (e.g., RQD) were applied to a blocky rock

Table 8 Field situations for the four study sites

Site no.	*RMR*	RMR_{mbi}	Field situation
1	40.10 (III)	42.18 (III)	Small rock blocks fall frequently; rock bolts and wire mesh are installed systematically, with shotcrete
2	49.39 (III)	36.19 (IV)	Rock blocks of different sizes fall frequently; rock bolts and wire mesh are installed systematically, with shotcrete
3	32.83 (IV)	18.56 (V)	Large-scale collapse occurs immediately after the excavation is completed; very long and dense rock bolts are installed systematically, with wire mesh and shotcrete of high thickness
4	42.34 (III)	64.41 (II)	Roadway roof is highly stable, and small blocks fall occasionally; local rock bolts are installed

Table 9 Rock mass ratings by stand-up time (mines) (Aksoy 2008)

Class mo.	I	II	III	IV	V
Average stand-up time	20 years for 15 m span	1 year for 10 m span	1 week for 5 m span	10 h for 2.5 m span	30 min for 1 m span

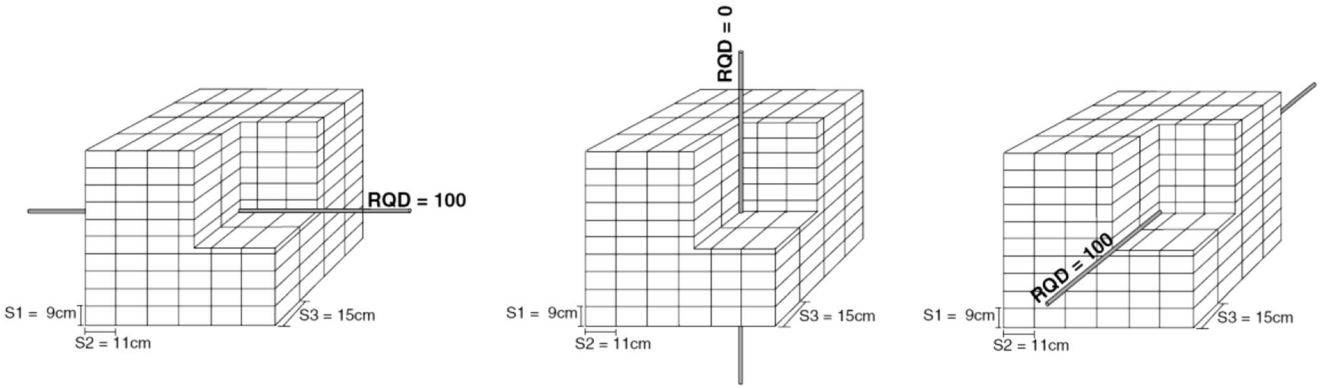

Fig. 34 Different *RQD* values with various directions (Palmstrom 2005). Note that S1, S2 and S3 are the average spacing of joint sets 1, 2 and 3, respectively

mass, various results could be experienced owing to different directions of the core drillings and scanlines, as shown in Fig. 34. Zheng et al. (2018) also used an example to demonstrate that for a stratified rock mass, the *RQD* values rely heavily on borehole direction. Therefore, differences between R_{RQD+JF} and R_M are inevitable. However, three-dimensional measurements of rock mass jointing degree are not orientation-dependent (Palmstrom 2005). The MB_i is indeed a three-dimensional index, which is also a critical advantage of RMR_{mbi} compared to *RMR*.

Conclusions

Traditional measurements of block size or degree of jointing (e.g., *RQD*, *JF* and J_v) have been questioned and criticized, due to their inherent limitations, and the same is true for rock mass classification systems. Therefore, in this study, the MB_i was introduced, and correlations of MB_i with *RQD*, *JF* and J_v were evaluated; the combined use of *RQD* and *JF* was replaced with MB_i in the *RMR* system, and this version was termed RMR_{mbi}. From the results, the following conclusions can be drawn:

(i) Close correlations were found between MB_i and *RQD*, *JF* and J_v, and when joint persistence was considered, the correlations were more significant, which shows that the MB_i can fully capture the influence of joint persistence. Based on these correlations, the reasonableness and advantages of MB_i are highlighted.

(ii) Because of the lack of sufficient real applications of RMR_{mbi} (which is also a limitation of this study), simulated experiments were conducted to confirm the viability of RMR_{mbi}, and the experimental results were in line with the objective trends (Section 3.2). Experimental simulation results suggest that the sensibility of R_M and R_{RQD+JF} is similar, but R_M is better because it can properly distinguish rock masses whose jointing ratings are

lower than 8 (Fig. 22). Comparative analysis of RMR_{mbi} and RMR shows that in some cases, RMR_{mbi} is the same as RMR. The typical applications of RMR_{mbi} and RMR show that the RMR_{mbi} ratings are more in line with common practice, based on observations of field situations. For the relatively fractured rock masses, the RMR_{mbi} may be more reliable. Undoubtedly, the theoretical limitations of the combined use of RQD and JF are addressed, and the three-dimensional rock block sizes and joint persistence can be considered; therefore, the RMR_{mbi} system has strong application potential.

(iii) Compared to the RMR system, the RMR_{mbi} is simplified, because the RQD and JF are replaced with MB_i. To determine MB_i, the joint data and computer technology (presented in Section 2) are needed. However, in the short term, it is necessary to take time to complete the simulation of the joint system and calculation of block sizes, and the amount of time spent will be entirely dependent on the complexity of the joint system.

Additionally, the RMR_{mbi} developed in this study is a new offering. In future work, significant effort should be made to further justify it, including (1) relations between RMR_{mbi} and various rock mass properties (e.g., rock mass strength); (2) stability assessment of different rock engineering properties (e.g., slope and tunnel) by supplementing the RMR_{mbi}; (3) determining how to select proper supporting schemes based on RMR_{mbi}; and (4) determining how to rapidly simulate the rock joint system and calculate the rock block sizes for determining an RMR_{mbi} value within a short period of time.

Acknowledgements This work was funded by the National Key R&D Program of China (no. 2018YFC0808402).

Compliance with ethical standards

Conflict of interest The authors declare no conflict of interest.

References

Aksoy CO (2008) Review of rock mass rating classification: historical developments, applications, and restrictions. J Min Sci 44:51–63. https://doi.org/10.1007/s10913-008-0005-2

Aydan Ö, Ulusay R, Tokashiki N (2014) A new rock mass quality rating system: rock mass quality rating (RMQR) and its application to the estimation of geomechanical. Rock Mech Rock Eng 47:1255–1276. https://doi.org/10.1007/s00603-013-0462-z

Barton N, Lien R, Lunde J (1974) Engineering classification of rock masses for the design of tunnel support. Rock Mech Felsmechanik Mécanique des Roches 6:189–236. https://doi.org/10.1007/BF01239496

Bejari H, Khademi Hamidi J (2013) Simultaneous effects of joint spacing and orientation on TBM cutting efficiency in jointed rock masses. Rock Mech Rock Eng 46:897–907. https://doi.org/10.1007/s00603-012-0314-2

Bieniawski ZT (1989) Geomechanics classification: engineering rock mass classifications. Wiley, New York

Buyer A, Schubert W (2017) Calculation the spacing of discontinuities from 3D point clouds. Procedia Eng 191:270–278. https://doi.org/10.1016/j.proeng.2017.05.181

Celada B, Tardáguila I, Varona P, Bieniawski ZT (2014) Innovating tunnel design by an improved experience-based RMR system. In: Proceedings of the World Tunnel Congress 2014 – Tunnels for a better Life. Foz do Iguaçu, Brazil, vol 3, pp 1–9

Central South University, Huaxi Group, Liuzhou Huaxi Nonferrous Designing Institute (2011) Assessment of the engineering rock mass quality in Xintongkuang mine (a concluding report)

Chen Q, Niu W, Zheng W et al (2018) Correction of some problems in blockiness evaluation method in fractured rock mass. Rock Soil Mech 39(10):3727–3734 (in Chinese with English abstract)

Chen Q, Yin T, Jia H (2019) Selection of optimal threshold of generalised rock quality designation based on modified blockiness index. Advances in Civil Engineering 2019:1340549

Deere DU, Hendron AJ, Patton FD et al (1967) Design of Surface and Near-Surface Construction in rock. In: Fairhurst C (ed) Failure and breakage of rock. Society of Mining Engineers of AIME, New York, pp 237–302

Dershowitz W, Doe T, Uchida M et al (2003) Correlations between fracture size, transmissivity, and aperture. Soil and rock America. In: Proceedings of the 12th Panamerican Conference on Soil Mechanics and Geotechnical Engineering, 39th US Rock Mechanics Symposium, Cambridge, 22-26 June, pp 887–891

Feng X, Jimenez R (2015) Estimation of deformation modulus of rock masses based on Bayesian model selection and Bayesian updating approach. Eng Geol 199:19–27. https://doi.org/10.1016/j.enggeo.2015.10.002

Grenon M, Hadjigeorgiou J (2003) Evaluating discontinuity network characterization tools through mining case studies. Soil Rock America 2003, Boston, 1, 137–142

Guangxi University, Huaxi Group (2013) Classification for the jointed rock masses and optimization of the mining technology in Tongkeng mine (a concluding report)

Harrison JP (1999) Selection of the threshold value in RQD assessments. Int J Rock Mech Min Sci 36:673–685

Hoek E, Diederichs MS (2013) Quantification of the geological strength index chart. Presented at the 47th US Rock Mechanics/Geomechanics Symposium, ARMA 13-672, San Francisco CA, June 23-26, 2013

ISRM (1978) Suggested methods for the quantitative description of discontinuities in rock masses. Int J Rock Mech Min Sci Geomech Abstr 15:319–368. https://doi.org/10.1016/0148-9062(79)91476-1

Itasca (2013) 3DEC: three-dimensional distinct element code. Ver. 5.0. Itasca Consulting Group Inc, Minneapolis

Kim BH, Cai M, Kaiser PK, Yang HS (2007) Estimation of block sizes for rock masses with non-persistent joints. Rock Mech Rock Eng 40:169–192. https://doi.org/10.1007/s00603-006-0093-8

Koutsoftas DC (2017) Discussion of "rock quality designation (RQD): time to rest in peace". Can Geotech J 55:584–592. https://doi.org/10.1139/cgj-2017-0497

Li Y, Wang Q, Chen J et al (2014) Determination of structural domain boundaries in jointed rock masses: an example from the Songta dam site, China. J Struct Geol 69:179–188

Lin F (2008) Evaluation of in-situ measurement methods for counting volumetric joints of rock mass. J Eng Geol 16:663–666 (in Chinese with English abstract)

Liu Q, Liu J, Pan Y et al (2017) A case study of TBM performance prediction using a Chinese rock mass classification system – hydropower classification (HC) method. Tunn Undergr Sp Technol 65:140–154. https://doi.org/10.1016/j.tust.2017.03.002

Martin MW, Tannant DD (2004) A technique for identifying structural domain boundaries at the EKATI diamond mine. Eng Geol 74:247–264. https://doi.org/10.1016/j.enggeo.2004.04.001

Miller SM (1983) A statistical method to evaluate homogeneity of structural populations. Math Geol 15:317–328

Palmstrom A (1982) The volumetric joint count: a useful and simple measure of the degree of rock mass jointing. Proc 4th Congr Int Assoc, Engng Geol, vol 2, pp 221–228

Palmstrom A (1996) Characterizing rock masses by the RMi for use in practical rock engineering: part 1: the development of the rock mass index (RMi). Tunn Undergr Sp Technol 11:175–188. https://doi.org/10.1016/0886-7798(96)00015-6

Palmstrom A (2005) Measurements of and correlations between block size and rock quality designation (RQD). Tunn Undergr Sp Technol 20:362–377. https://doi.org/10.1016/j.tust.2005.01.005

Pan H (2012) Research on grouting uplifting mechanism of plinth of concrete facing dam. Xihua University, Chengdu

Pells PJ, Bieniawski ZT, Hencher SR, Pells SE (2017) Rock quality designation (RQD): time to rest in peace. Can Geotech J 54:825–834. https://doi.org/10.1139/cgj-2016-0012

PRC Ministry of Construction (1995) Standard for engineering classification of rock masses. China planning press, China (in Chinese)

Priest SD, Hudson JA (1976) Discontinuity spacings in rock. Int J Rock Mech Min Sci 13:135–148. https://doi.org/10.1016/0148-9062(76)90818-4

Riquelme AJ, Abellán A, Tomás R (2015) Discontinuity spacing analysis in rock masses using 3D point clouds. Eng Geol 195:185–195. https://doi.org/10.1016/j.enggeo.2015.06.009

Riquelme AJ, Tomás R, Abellán A (2016) Characterization of rock slopes through slope mass rating using 3D point clouds. Int J Rock Mech Min Sci 84:165–176. https://doi.org/10.1016/j.ijrmms.2015.12.008

Shang J, West LJ, Hencher SR, Zhao Z (2018) Geological discontinuity persistence: implications and quantification. Eng Geol 241:41–54. https://doi.org/10.1016/j.enggeo.2018.05.010

Terzaghi RD (1965) Sources of error in joint surveys. Géotechnique 15:287–304. https://doi.org/10.1680/geot.1965.15.3.287

Wang X (2011) Analysis and simulation of fractured character in layer rockmass based on probabilistic: a case study of the dam of Jinping I hydropower station. China University of Geoscience, Wuhan

Wang C, Hu P, Sun W (2010) Method for evaluating rock mass integrity based on borehole camera technology. Rock Soil Mech 31:1326–1330. (in Chinese with English abstract). https://doi.org/10.16285/j.rsm.2010.04.008

Warren SN, Kallu RR, Barnard CK (2016) Correlation of the rock mass rating (RMR) system with the unified soil classification system (USCS): introduction of the weak rock mass rating system (W-RMR). Rock Mech Rock Eng 49:4507–4518. https://doi.org/10.1007/s00603-016-1090-1

Wong LNY, Lai VSK, Tam TPY (2018) Joint spacing distribution of granites in Hong Kong. Eng Geol 245:120–129. https://doi.org/10.1016/j.enggeo.2018.08.009

Xia L, Li M, Chen Y et al (2015) Blockiness level of rock mass around underground powerhouse of three gorges project. Tunn Undergr Sp Technol 48:67–76. https://doi.org/10.1016/j.tust.2015.02.002

Xia L, Zheng Y, Yu Q (2016) Estimation of the REV size for blockiness of fractured rock masses. Comput Geotech 76:83–92. https://doi.org/10.1016/j.compgeo.2016.02.016

Yarahmadi R, Bagherpour R, Taherian SG, Sousa LMO (2018) Discontinuity modelling and rock block geometry identification to optimize production in dimension stone quarries. Eng Geol 232:22–33. https://doi.org/10.1016/j.enggeo.2017.11.006

Zhang L (2016) Determination and applications of rock quality designation (RQD). J Rock Mech Geotech Eng 8:389–397. https://doi.org/10.1016/j.jrmge.2015.11.008

Zhang Q, Bian Z, Yu M (2009) Preliminary research on rockmass integrity using spatial block identification technique. Yanshilixue Yu Gongcheng Xuebao/Chinese J Rock Mech Eng 28(3):507–515 (in Chinese with English abstract)

Zhang W, Wang Q, Chen J et al (2012) Determination of the optimal threshold and length measurements for RQD calculations. Int J Rock Mech Min Sci 51:1–12

Zhang W, Chen J, Cao Z, Wang R (2013) Size effect of RQD and generalized representative volume elements: a case study on an underground excavation in Baihetan dam, Southwest China. Tunn Undergr Sp Technol 35:89–98. https://doi.org/10.1016/j.tust.2012.12.007

Zheng J, Deng J, Yang X et al (2014) An improved Monte Carlo simulation method for discontinuity orientations based on fisher distribution and its program implementation. Comput Geotech 61:266–276

Zheng J, Yang X, Lü Q et al (2018) A new perspective for the directivity of rock quality designation (RQD) and an anisotropy index of jointing degree for rock masses. Eng Geol 240:81–94. https://doi.org/10.1016/j.enggeo.2018.04.013